Parameterization of the Evaporation of Rainfall for Use in General Circulation Models

GRAHAM FEINGOLD

Cooperative Institute for Research in Environmental Sciences, University of Colorado, Boulder, Colorado

(Manuscript received 7 May 1992, in final form 8 April 1993)

ABSTRACT

A parameterization of evaporation losses below cloud base is presented for use in general circulation models to assist in quantification of water content in the hydrological cycle. The scheme is based on detailed model calculations of the evolution of raindrop spectra below cloud base and includes the processes of collision coalescence/breakup. Evaporation is expressed as a percentage decrease in the liquid water mixing ratio, and the parameterization is formulated as an algebraic equation in (i) the cloud-base values of the mixing ratio and the drop concentration, (ii) the fall distance, and (iii) the lapse rate of temperature in the subcloud environment. Results show that when compared to the detailed model calculations, good estimates of evaporation (usually within 20% and often within 10%) are obtained for a wide range of conditions. An analysis of the errors in evaporation calculations associated with errors in the parameterization variables is performed.

1. Introduction

The impact of clouds on climate is more and more frequently cited as a first priority in climate studies (e.g., Committee on Earth Sciences 1989). Clouds are usually considered in terms of their effect on radiative transfer in the earth's atmosphere; however, the precipitation they produce is also an important part of the hydrological cycle. A number of general circulation models (GCMs) are being used to study the earth's atmosphere as well as the role of clouds in this complex system (e.g., the 14 models described by Cess et al. 1989). Clouds are invariably subgrid-scale features in GCMs, and their parameterization has proved to be a formidable task; consequently, the parameterization schemes that represent clouds in GCMs are still somewhat crude.

While in recent years many studies have focused on clouds and cloud processes in relation to climate (e.g., Slingo 1987; Mitchell et al. 1989; Smith 1990), the rainfall produced by these clouds has not received the same level of attention. The ability of a cloud to produce precipitation will determine the optical properties of that cloud by affecting the extent of the cloud, the liquid (ice) water content, and the hydrometeor size. The latter will, in turn, affect the rate of rainfall evaporation below cloud base. Precipitation also affects soil moisture (which affects vegetation), and sea surface salinity and temperature (Browning 1990). There is an obvious need to include rainfall processes in GCMs in as realistic a manner as possible.

Corresponding author address: Dr. Graham Feingold, CIRES, Campus Box 449, University of Colorado, Boulder, CO 80309-0449.

This paper will limit itself to the problem of rainfall evaporation. Sundqvist (1978) and, more recently, Schlesinger et al. (1988, henceforth SOR) presented parameterization schemes, designed for use in GCMs, that describe the evaporation of rain below cloud base. Both of these schemes were based on theoretical and semiempirical considerations and require specific parameters to quantify the degree of evaporation. Sundqvist (1978) determined the parameter arbitrarily whereas SOR used radar measurements of precipitation losses (from continental convective clouds) in order to estimate their parameters. Here we will quantify the evaporation of precipitation below cloud base in a more general fashion, by studying the problem for situations analogous to different cloud types and a variety of atmospheric conditions.

The basis for this parameterization is a numerical modeling study. Although numerical models are invariably an abstraction of nature, they do provide a convenient means of studying physical problems in a self-consistent framework; parameters can be changed to check their effect on the system, and hypotheses can be put to test. Ultimately, it is desirable to formulate a parameterization scheme based on both numerical studies and observations. Viewed in this light, the parameterization presented here might be regarded as *qualitative,* despite the fact that it presents *quantitative* estimates of precipitation evaporation. On this note, however, it should be mentioned that a previous study (Levin et al. 1991) that compared raindrop spectral evolution as measured along a mountain slope in Switzerland with results from a model similar to the one employed here was sufficiently favorable so as to provide confidence that this model adequately simulates the evaporation of natural precipitation.

In formulating this parameterization, I have attempted to account for the most important parameters affecting raindrop evaporation. The choice of parameters emanates from a number of rainfall studies that have appeared in the literature over the past years. The list of works (by no means exhaustive) includes those of Kamburova and Ludlam (1966), Clark and List (1971), Girard and List (1975), Srivastava (1985), Proctor (1988), and Feingold et al. (1991). These works have pointed to the importance of macroscale properties such as fall distance, lapse rate of temperature, and cloud-base temperature, as well as microscale properties, namely, the drop size spectrum at cloud-base.

In section 2, the model used in this study is briefly described, and the method of generating the parameterization scheme is discussed. Section 3 presents the model results for a wide range of conditions. Section 4 discusses ways of implementing the scheme in GCMs, as well as some of the assumptions adopted in generating the scheme.

2. Method

a. The model

The calculations are based on the modeling studies of Tzivion et al. (1989) and Feingold et al. (1991). Great attention is placed on the microphysical processes, as well as on calculations of the saturation field. Feingold et al. (1991) used a two-dimensional, axisymmetrical model to study the effect of evaporation on the generation of downdrafts. In the current study a one-dimensional version of that model is used. Although it is recognized that the problem is essentially a three-dimensional one, the reader will appreciate that to generate a parameterization scheme of this nature, a very large number of calculations must be performed. Given the present resolution of GCMs (about 300 km in the horizontal), it seems reasonable at the present time to study the problem in a one-dimensional (that is, vertical) sense.

The rainfall–atmosphere system is a coupled system in which dynamical and microphysical processes are closely related; the environment in which a drop is located affects its rate of evaporation, and the evaporation rate affects the dynamical fields. The model equations are briefly adumbrated; further details are furnished in Feingold et al. (1991). The symbols used in the model equations are defined in the Appendix. The equation for vertical velocity w' is given by

$$\frac{\partial w'}{\partial t} = F(w') + D(w') + g\left(\frac{\theta_v'}{\theta_{v0}} - X_l\right). \quad (1)$$

The equations for the virtual temperature perturbation θ_v' and vapor mixing ratio perturbation q_v' are

$$\frac{\partial \theta_v'}{\partial t} = F(\theta_v') + D(\theta_v') + \Gamma_{\theta 0} w' + L/c_p[(\delta X_l)_{\text{cond/evap}}(P_0/P)^{R_d/c_p}] \quad (2)$$

$$\frac{\partial q_v'}{\partial t} = F(q_v') + D(q_v') + \Gamma_{q0} w' - (\delta X_l)_{\text{cond/evap}}. \quad (3)$$

We include an explicit, 33-bin representation of the drop size spectrum and solve the kinetic equations for droplet collisional coalescence/breakup and condensation/evaporation (cond/evap) using the method of moments (Tzivion et al. 1989). The accuracy of this method makes it compatible for studying drop size–sensitive processes such as evaporation. We therefore require dynamic equations for both bin number N_k and bin mass M_k, 66 equations in all:

$$\frac{\partial N_k}{\partial t} = F(N_k) + D(N_k) + \frac{\delta N_k}{\delta t_{\text{evap}}} + \frac{\delta N_k}{\delta t_{\text{coll}}} \quad (4)$$

$$\frac{\partial M_k}{\partial t} = F(M_k) + D(M_k) + \frac{\delta M_k}{\delta t_{\text{evap}}} + \frac{\delta M_k}{\delta t_{\text{coll}}}. \quad (5)$$

(The subscript "coll" refers to collisional processes.) The turbulent diffusion operator $F(\phi)$ and advection operator $D(\phi)$ in equations (1)–(5) are, respectively,

$$F(\phi) = K\frac{\partial^2 \phi}{\partial z^2} \quad (6)$$

$$D(\phi) = -w'\frac{\partial \phi}{\partial z}. \quad (7)$$

In the present study, as in other one-dimensional studies (e.g., Srivastava 1985), the force derived from the pressure perturbation is neglected in the equation in w'. This makes the system of equations more applicable to convective downdrafts than widespread rain. It will also be assumed that there is no turbulent diffusion; that is, $K = 0$. The implication is that we do not treat entrainment of environmental air into the rain shaft. Inclusion of entrainment would go beyond the scope of this study but could be included at a later stage (see discussion in section 4). The grid size is set at 20 m to minimize the numerical diffusion associated with the forward, upstream advection scheme used to solve (7).

The model is initiated by prescribing initial profiles of temperature and vapor mixing ratio together with a source of precipitation (that is, a size spectrum of drops) at cloud base (z = 2000 m). From cloud base to the top of the model (z = 2200 m), a saturated environment with zero thermal buoyancy is prescribed.

b. Basic parameters

Various studies of rainfall evaporation have pointed to the importance of a number of parameters. These include the following.

1) DROP SIZE

The rate of evaporation of drops is a strong function of drop size. Drop spectra comprising a large number of small drops will be more susceptible to evaporation than the same amount of water distributed amongst larger drops. As a result, all microphysical processes that affect drop size should be considered. For warm rainfall these include evaporation and collisional coalescence/breakup. Srivastava (1985) and SOR made the same assumption that the effects of coalescence and breakup cancel one another, whereas Feingold et al. (1991) included these effects. Here too, we include coalescence and breakup, and the severity of neglecting these processes is ascertained (see section 3).

Model runs are performed using input spectra of the lognormal form, expressed in terms of the liquid water mixing ratio X_{l0} [g g^{-1}] and number concentration N_{t0} [cm^{-3}] of the drops. (The subscript "0" implies the values at cloud base.) A constant breadth of the size spectrum is assumed, based on the observational study of Feingold and Levin (1986). The lognormal distribution has been shown by many (e.g., Levin 1954; Feingold and Levin 1986) to provide a good fit to observed drop spectra. The parameter X_{l0} is varied over the range of values 0.5×10^{-3} to 2.0×10^{-3} in increments of 0.5×10^{-3}, while N_{t0} is varied from 10^2 cm^{-3} to 10^{-3} cm^{-3} in logarithmic decrements of 10^{-1} cm^{-3}. These values adequately cover those observed under a wide range of precipitation conditions.

2) LAPSE RATE OF TEMPERATURE, CLOUD-BASE TEMPERATURE, AND RELATIVE HUMIDITY OF THE SUBCLOUD LAYER

We consider well-mixed subcloud layers where the vapor mixing ratio q_v is constant with height. In such a case, the cloud-base temperature T_b determines the value of q_v (assuming cloud base is at 100% relative humidity). A constant value of q_v is consistent with the trend for relative humidity to increase from values at the ground to 100% at cloud base. The profile of relative humidity below the cloud is determined by T_b and lapse rate of temperature γ.

Various works (e.g., Harris 1977; Srivastava 1985; Proctor 1988; Feingold et al. 1991) have demonstrated that γ has a strong impact on the generation of downdrafts, with w' increasing as γ approaches its dry-adiabatic value of Γ_d. The magnitude of w' affects the thermodynamic fields and the spatial distribution of the rainfall, and, consequently, the evaporation rates; w' also affects evaporation by placing a constraint on the time available for evaporation. In the model simulations, the lapse rate of temperature is varied from 7.5°C km^{-1} to 9.5°C km^{-1} in increments of 1°C km^{-1}. Cloud-base temperature is fixed at either 5°C or 10°C, and at an altitude of 2 km.

c. Multivariate regressions

Because of the vast number of calculations performed by GCMs, it is imperative that the parameterization scheme require a minimum of computation time. This dictates a compromise between a highly desirable level of accuracy, which would require significant computation time, and a realistically achievable level of accuracy, which would require a modest amount of time. We sought to achieve a parameterization scheme that requires very low computation time, without a significant compromise in accuracy.

This parameterization scheme estimates the percentage decrease in water mixing ratio X_l and will be expressed in terms of the following important parameters discussed above:

(i) liquid water mixing ratio at cloud base, X_{l0} [g g^{-1}],
(ii) number concentration of drops water at cloud base, N_{t0} [cm^{-3}],
(iii) distance of fall below cloud base, h [m], and
(iv) lapse rate of temperature, γ [°C km^{-1}].

An additional important parameter, w', has not been included because of the difficulty of calculating subgrid-scale vertical velocities in GCMs. The parameters X_{l0} and γ alleviate this to some extent, because together they control the magnitude of the downdraft (e.g., Srivastava 1985). The results will show that despite the fact that w' is not explicit in the parameterization scheme, good estimates of evaporation are obtained for a broad range of conditions (see section 3).

We define the percentage loss in X_l as

$$E(X_{l0}, N_{t0}, h, \gamma) = [(X_{l0} - X_l(h))/X_{l0}]100. \quad (8)$$

It is necessary to obtain a valid functional form for the left-hand side of (8), bearing in mind the computation time constraints imposed by large-scale models. The model equations (1)–(5) provide little assistance in this matter due to the complexity of the dynamical and microphysical processes under consideration. On the other hand, the analytical model of SOR is valuable in this regard. SOR formulated their parameterization in terms of the gamma size distribution of raindrops. They used an analytical model based on a simplified set of equations, which expresses the decrease in rain rate as a function of fall distance as follows:

$$I_0(0) - I_0(h) = CI_0^{\alpha}(0)\Psi(h). \quad (9)$$

(For details, see SOR.) $I_0(h)$ is the rain rate at fall distance h; C and α are coefficients dependent (amongst others) on the drop size distribution parameters; and $\Psi(h)$ is a function related to the subcloud saturation ratio, temperature profile, as well as other thermodynamical constants associated with drop evaporation. Note that the general definition for rain rate I is

$$I = \frac{4}{3}\pi \int_0^\infty [v(r) - w']r^3 n(r)dr \qquad (10)$$

with $n(r)dr$ the number of drops per unit volume with sizes between r and $r + dr$ and $v(r)$ the terminal fall velocity of a drop of radius r. SOR assumed $w' = 0$ in (10), hence the use of the subscript 0 in (9).

Schlesinger et al. showed how C is a power-law function of drop concentration N_t. (This is true for common representations of the drop spectrum such as gamma, lognormal, and exponential distributions.) In addition, it is easy to show that the function $\Psi(h)$ is very well approximated by a power-law dependence on both h and γ. (The latter is valid for atmospheres with both constant vapor mixing ratio profiles and constant relative humidity profiles.) Although SOR developed these relationships for rain rate I_0, they are also valid (in terms of their functional dependencies) for X_l, since by definition,

$$X_l = \frac{4}{3}\pi \frac{\rho_l}{\rho_a} \int_0^\infty r^3 n(r)dr \qquad (11)$$

(ρ_l is the density of liquid water). The analogy between I_0 and X_l is straightforward when a power-law dependence of $v(r)$ on r is assumed in (10) (e.g., Rogers and Yau 1989). Thus, we will avail ourselves of the SOR analytical model and propose a functional dependence of $E(X_{l0}, N_{t0}, h, \gamma)$ of the form:

$$E(X_{l0}, N_{t0}, h, \gamma) = a_0 X_{l0}^{a_1} N_{t0}^{a_2} h^{a_3} \gamma^{a_4}, \quad (12a)$$

where a_i are the regression coefficients. Multivariate linear regressions were performed on the logarithm of the model produced data in order to produce the coefficients in Eq. (12a). Equation (12a) can on occasion generate values of E greater than 100%, necessitating the constraint that

$$E \leqslant 100\%. \qquad (12b)$$

Equation (12) will henceforth be referred to as PF. Note that we have assumed that because the power-law form (12a) is valid for SOR's analytical model, it is also valid for the more detailed set of equations (1)–(5). We do not offer rigorous proof for the validity of this form, only that model simulations verify its suitability and that it provides good accuracy (usually within 20%, and often within 10%) over a broad range of conditions. Furthermore, functions of a relatively simple form are advantageous when computing time is at a premium. A similar approach was used successfully by Feingold and Heymsfield (1992) for parameterizing condensation.

Similar to Sundqvist (1978) and SOR, the proposed empirical equation (12) requires a number of coefficients to quantify the evaporation. Here, we provide model-derived estimates of these coefficients for a wide range of conditions.

3. Results

Model runs were repeated for the range of X_{l0}, N_{t0}, and γ described in section 2. In each case, the drop spectrum was used as a source at cloud base and a run was terminated when a steady state of the various fields had been established. This resulted in a total of 72 model runs (7200 data points) for each parameterization (one at $T_b = 5°C$ and another at $T_b = 10°C$). An additional set of 72 runs was performed excluding collision coalescence/breakup to evaluate the importance of these processes. Additional experiments would be desirable, but with typical time requirements of 15 min CPU (per run) on a CRAY Y/MP, these had to be limited.

a. Estimates of evaporation rates including collision coalescence/breakup for $T_b = 5°C$

The regression produces the coefficients a_i required by (12). Table 1 summarizes the values of the five parameters, a_0, a_1, a_2, a_3, and a_4. Also shown are the parameters a_0 through a_3 for the individual cases of $\gamma = 7.5$, 8.5, and 9.5 [°C km^{-1}]. In all cases the standard error of estimate (SEE) is low enough to signify a good overall fit of the regression equation to the model-generated data.

1) $\gamma = 7.5°C\ km^{-1}$

Figure 1 presents contours of E generated by the model for the case $\gamma = 7.5°C\ km^{-1}$ for fall distances of (a) 500 m, (b) 1000 m, (c) 1500 m, and (d) 2000 m in $(N_{t0}; X_{l0})$ space. As anticipated by previous studies, there is a tendency for evaporation to increase with (i) increasing drop concentration (for a given X_{l0}) and (ii) increasing fall distance. For a given value of N_{t0}, E decreases with increasing X_{l0} as increasing amounts of water are made available to humidify the atmosphere and inhibit evaporation. At low values of N_{t0} this latter trend is less marked because evaporation is slow and more water is still in the liquid, rather than the vapor, phase. An additional reason for the observed decrease

TABLE 1. The regression coefficients required by Eq. (12), that is $E(X_{l0}, N_0, h, \gamma) = a_0 X_{l0}^{a_1} N_{t0}^{a_2} h^{a_3} \gamma^{a_4}$ for $T_b = 5°C$ and various lapse rates of temperature, γ. The values are consistent with X_{l0} (in units of g g^{-1}), N_{t0} in cm^{-3}, h (in m), and γ (in °C km^{-1}); SEE is the standard error of estimate.

	All γ	$\gamma = 7.5°C\ km^{-1}$	$\gamma = 8.5°C\ km^{-1}$	$\gamma = 9.5°C\ km^{-1}$
a_0	0.00706	1.16	2.56	1.37
a_1	−0.0710	−0.0754	−0.0219	−0.0929
a_2	0.217	0.277	0.208	0.160
a_3	0.544	0.559	0.512	0.548
a_4	2.511			
SEE	14.8%	17.4%	11.6%	7.5%

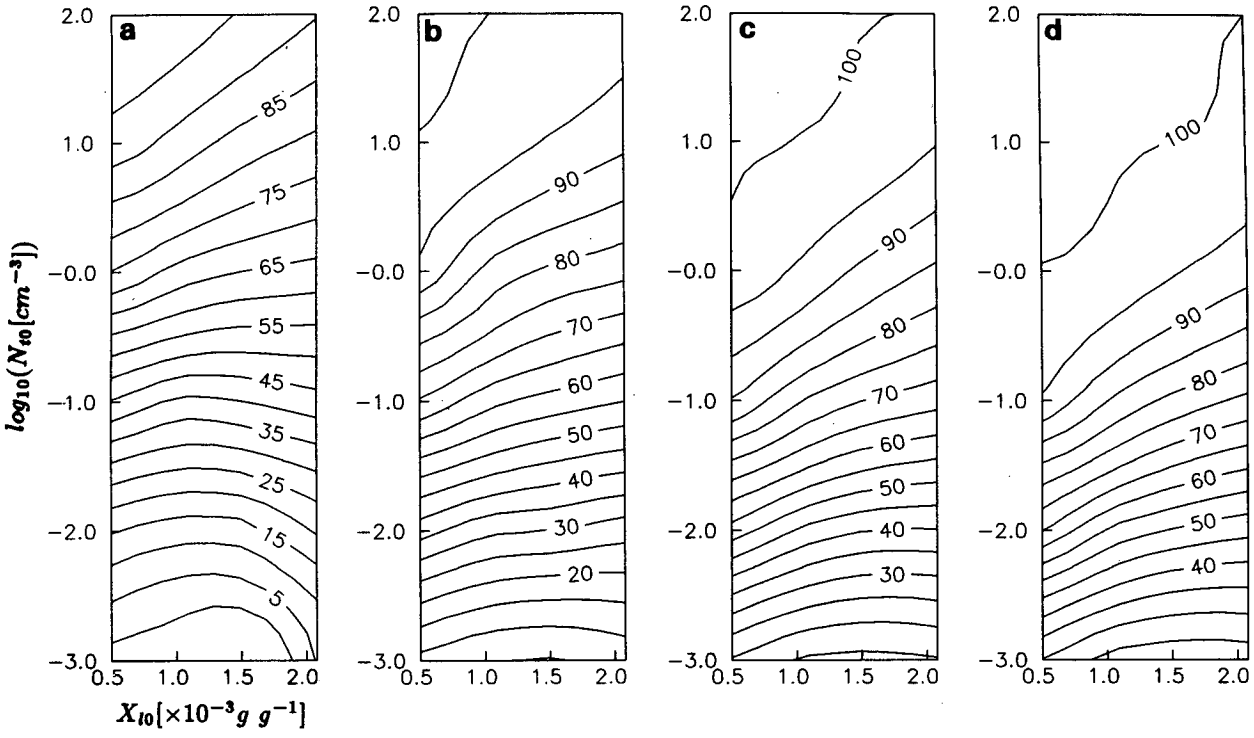

FIG. 1. Contours of the percentage decrease in liquid water mixing ratio (E) in (N_{l0}; X_{l0}) space as calculated by the model for fall distances of (a) 500 m, (b) 1000 m, (c) 1500 m, and (d) 2000 m. The lapse rate of temperature is 7.5°C km^{-1}.

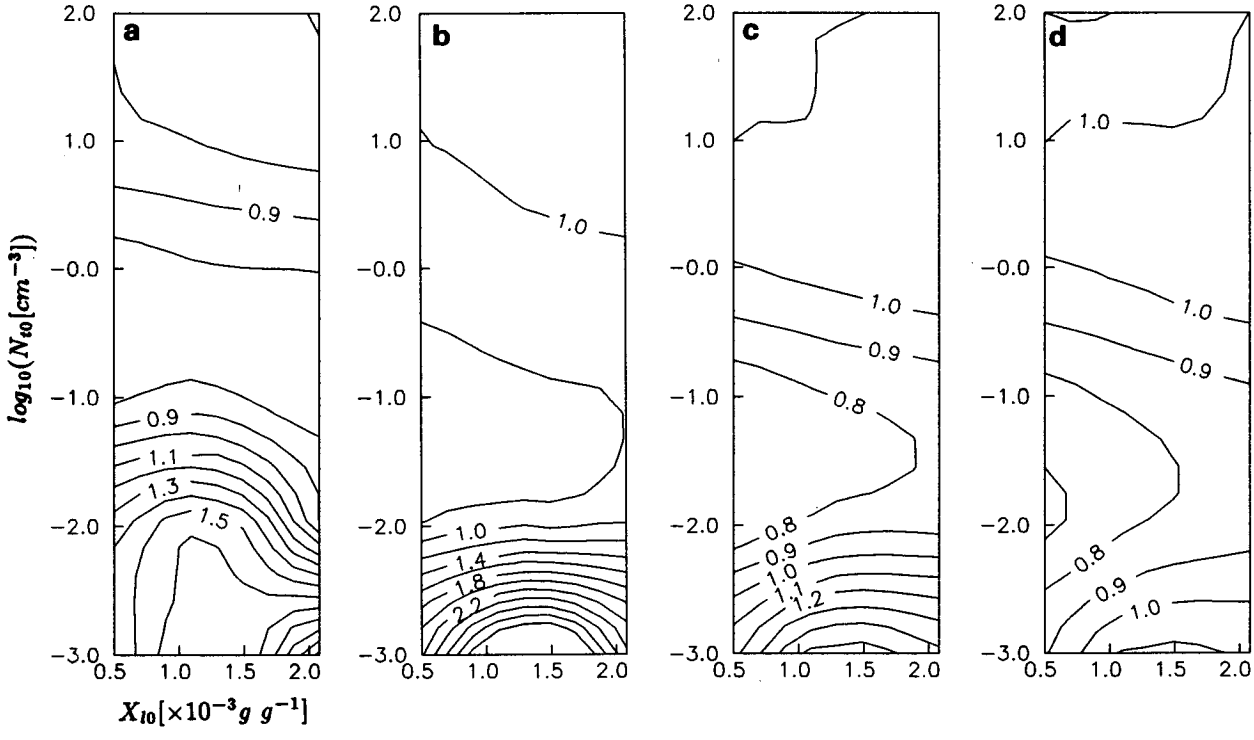

FIG. 2. Contours of the ratio of E as calculated by the parameterization scheme to E as calculated by the model in (N_{l0}; X_{l0}) space for fall distances of (a) 500 m, (b) 1000 m, (c) 1500 m, and (d) 2000 m. The lapse rate of temperature is 7.5°C km^{-1}.

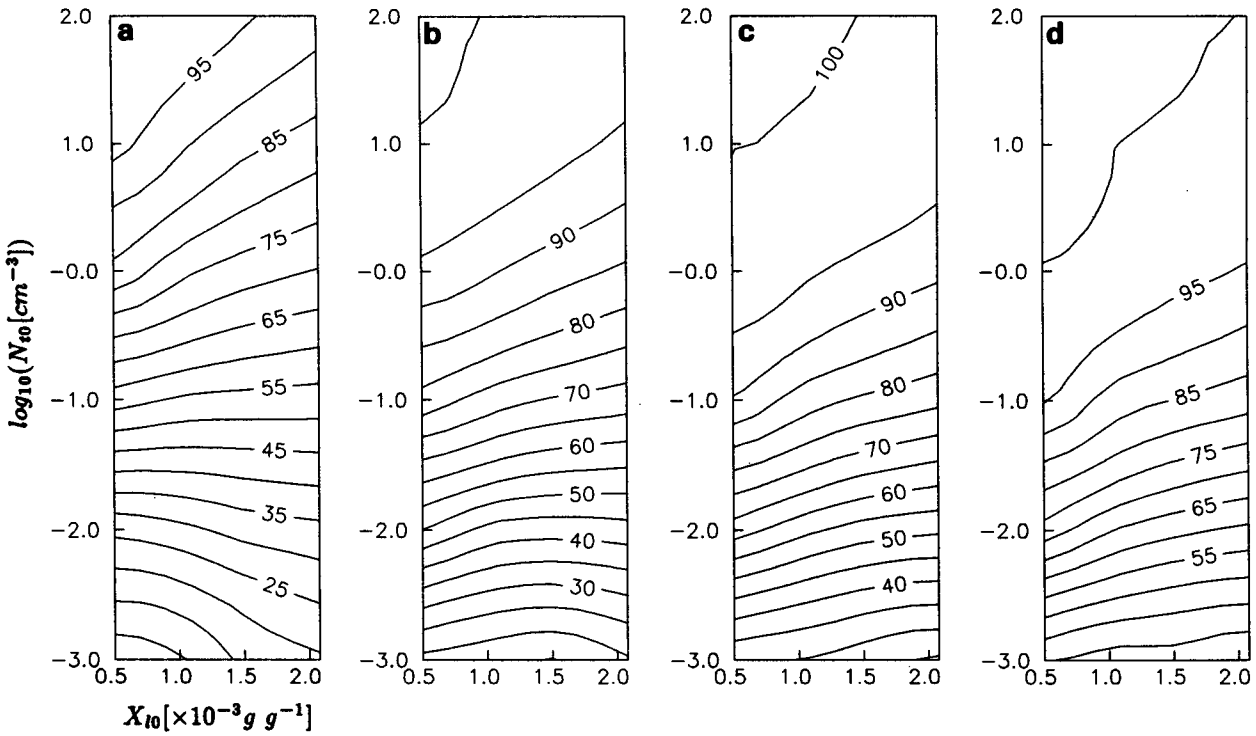

FIG. 3. As in Fig. 1 but for a lapse rate of 8.5°C km^{-1}.

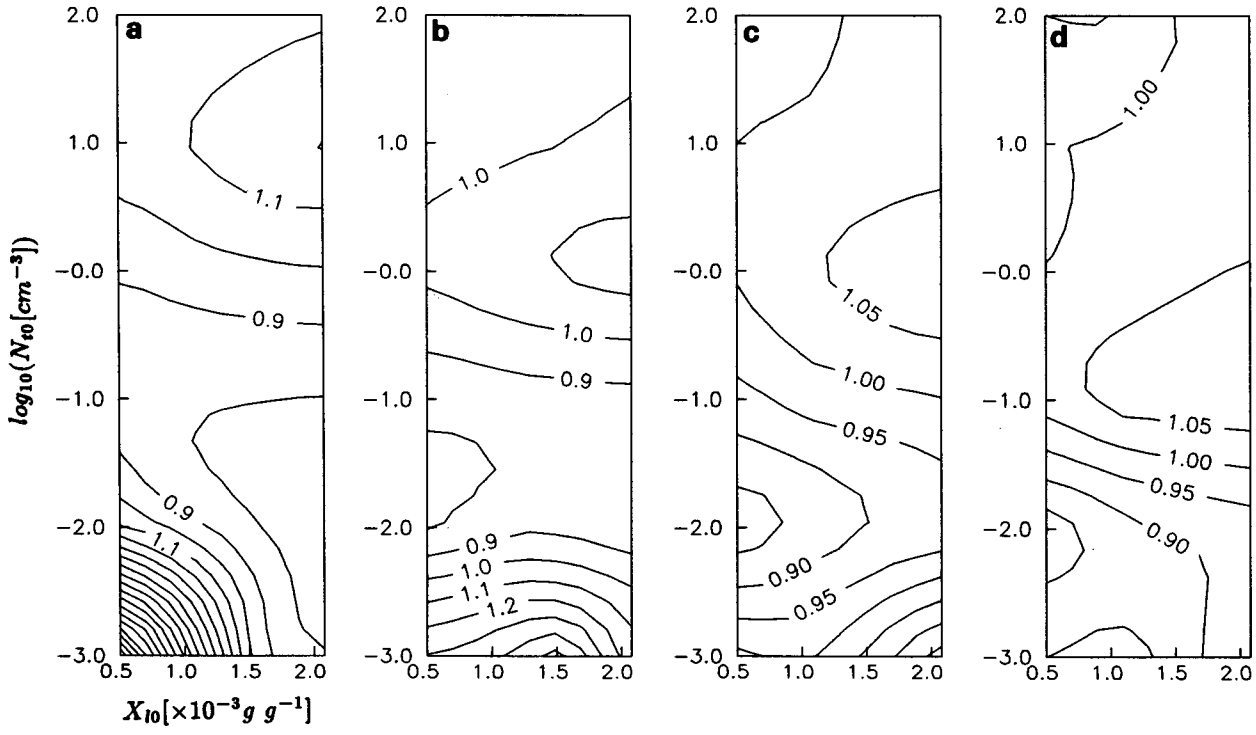

FIG. 4. As in Fig. 2 but for a lapse rate of 8.5°C km^{-1}.

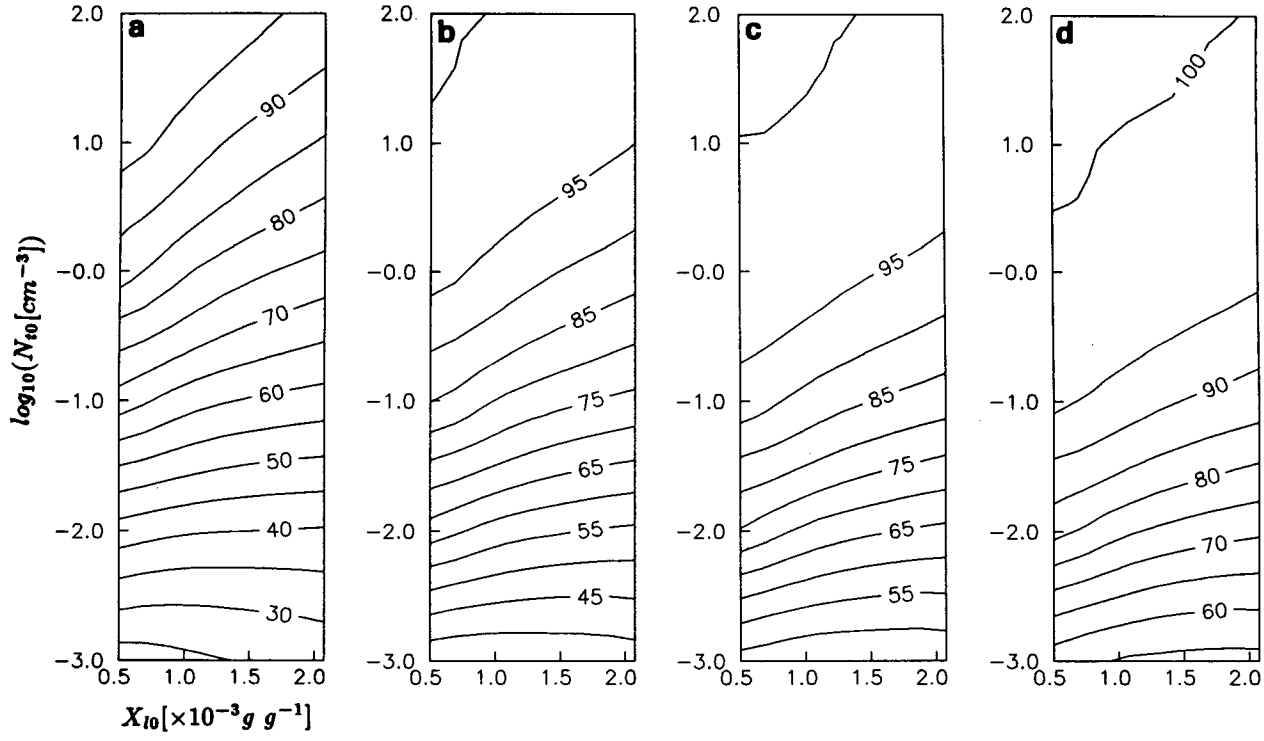

FIG. 5. As in Fig. 1 but for a lapse rate of 9.5°C km^{-1}.

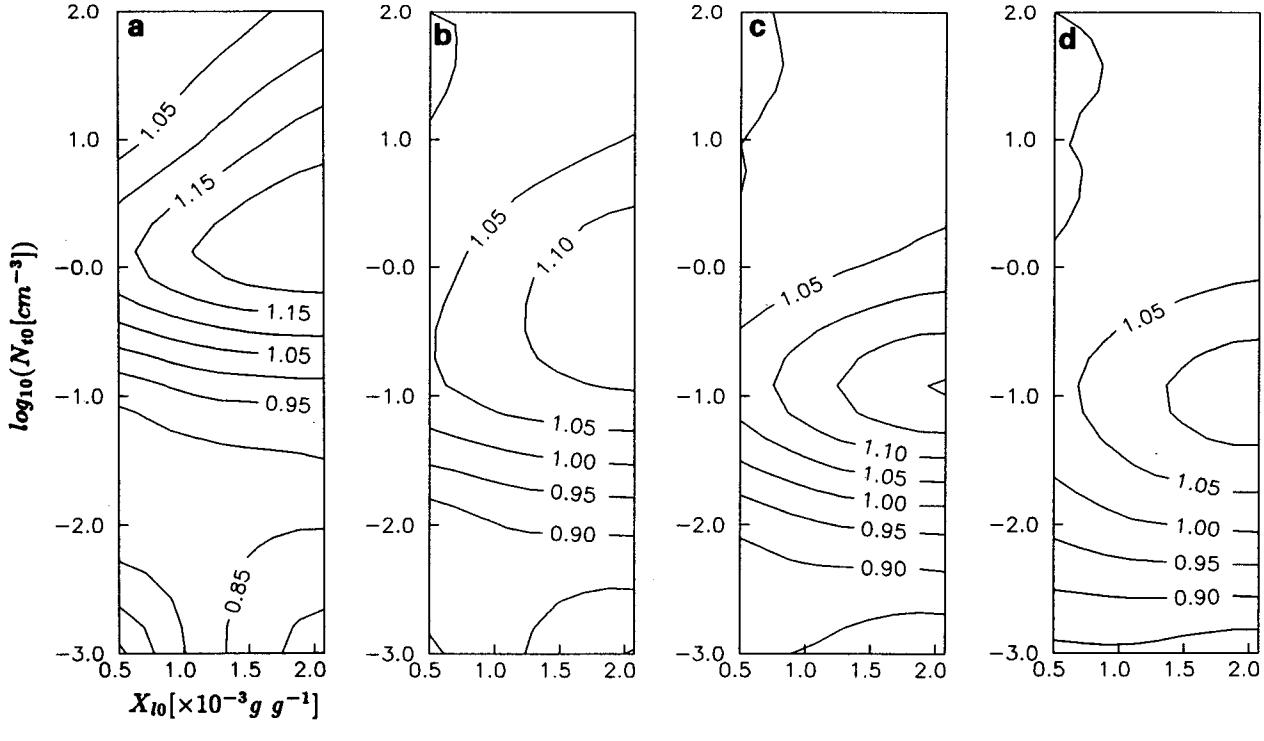

FIG. 6. As in Fig. 2 but for a lapse rate of 9.5°C km^{-1}.

in E with increasing X_{l0} (and constant N_{t0}) is due to the fact that higher X_{l0} will enhance downdraft development (through mass loading) and reduce the time available for evaporation. Figure 2 shows the ratio of the model-calculated values of E to values calculated using (12). Figure 2a shows that for a 500-m fall distance, PF is within 20% of the model results for $N_{t0} > 1.5 \times 10^{-2}$ and for all X_{l0}. At low N_{t0}, the results deteriorate rapidly; this is not of too great a concern because in this region, E is only of the order of 5% or 10% (Fig. 1a). As the fall distance increases (Figs. 2b–d), we see that accuracy rapidly improves, and the region of less than 20% error extends over a progressively larger area, until for $h = 2000$ m, it includes almost all the (N_{t0}; X_{l0}) space.

2) $\gamma = 8.5°C\ km^{-1}$

The results for $\gamma = 8.5°C\ km^{-1}$ (Figs. 3a–d) are qualitatively similar to those for $\gamma = 7.5°C\ km^{-1}$; however, evaporation rates are noticeably higher at low N_{t0}. This is because the drops are evaporating in a warmer, (relatively) drier environment and evaporation rates are too slow to offset this effect through cooling and moistening of the environment. At higher values of N_{t0}, the enhanced evaporation rates counter this effect.

There is a marked improvement in the results of PF relative to the model for $\gamma = 8.5°C\ km^{-1}$ (Figs. 4a–d). Although the region of gross overestimation of E evident in Fig. 2a can still be seen in Fig. 4a, it is confined to a smaller region. Increased fall distances (Figs. 4b–d) show progressively better results. At $h = 1000$ m, accuracy is better than 10% over the major part of the domain, whereas at $h = 2000$ m, it has improved to between 5% and 10% over the entire domain.

3) $\gamma = 9.5°C\ km^{-1}$

Similar results are obtained for the $\gamma = 9.5°C\ km^{-1}$ case with even higher evaporation rates at lower N_{t0} (Figs. 5a–d). The region of poor estimates of E visible in Figs. 2a and 4a has now been completely removed (Fig. 6a), and in general, PF produces good estimates of E throughout.

b. *Estimates of evaporation rates including collision coalescence/breakup for $T_b = 10°C$*

The results of PF for the case of $T_b = 10°C$ are summarized in Table 2. A comparison with the regression coefficients for the $T_b = 5°C$ case (Table 1) shows only small differences; therefore, the results are graphically depicted as a percentage difference (Δ_T) from the $T_b = 5°C$ case. Term Δ_T is defined as

$$\Delta_T = [(E_5 - E_{10})/E_5]100 \qquad (13)$$

with the subscripts 5 and 10, respectively, denoting T_b = 5°C and $T_b = 10°C$. Figure 7 shows the results for $\gamma = 8.5°C\ km^{-1}$ generated from the model output. We see that the percentage difference between the two cases ranges from about −1% at high N_{t0} to −6% at low N_{t0}. The negative values indicate a higher degree of evaporation in the warmer environment. At small N_{t0}, the evaporation rates are relatively slow and therefore more strongly influenced by the temperature increase than at large N_{t0}. For a given N_{t0}, the absolute value of Δ_T increases slightly with increasing X_{l0}; this is a consequence of the decrease in E_5 with increasing X_{l0} (see Fig. 3). The absolute value of Δ_T also tends to increase slightly with increasing h, which can be understood as the accumulated effect of the enhanced evaporation in the $T_b = 10°C$ case.

TABLE 2. The regression coefficients required by Eq. (12), that is, $E(X_{l0}, N_0, h, \gamma) = a_0 X_{l0}^{a_1} N_{t0}^{a_2} h^{a_3} \gamma^{a_4}$ for $T_b = 10°C$ and various lapse rates of temperature, γ. SEE is the standard error of estimate.

	All γ	$\gamma = 7.5°C\ km^{-1}$	$\gamma = 8.5°C\ km^{-1}$	$\gamma = 9.5°C\ km^{-1}$
a_0	0.0127	1.29	2.06	1.38
a_1	−0.0725	−0.0760	−0.0222	−0.0955
a_2	0.214	0.263	0.214	0.160
a_3	0.555	0.551	0.552	0.548
a_4	2.217			
SEE	13.7%	15.6%	11.8%	7.4%

c. *Estimates of evaporation rates excluding collision coalescence/breakup*

The set of 72 model runs excluding collision coalescence/breakup produces an equation in E of the form given by (12), with values of the parameters a_0, . . . , a_4 given in Table 3. Again, the regression coefficients are similar in sign and magnitude to those for the case with drop collisions (Table 1). Figure 8 shows a comparison of E for the two cases to evaluate the error introduced by excluding the drop collisions. The results (for $\gamma = 8.5°C\ km^{-1}$) are presented in terms of Δ_c, defined as

$$\Delta_c = [(E_{\text{incl}} - E_{\text{excl}})/E_{\text{incl}}]100 \qquad (14)$$

with the subscripts denoting inclusion (incl) and exclusion (excl) of drop collisions. Figure 8a shows that for $h = 500$ m, values of Δ_c vary from about −0.5% at high N_{t0} up to about 4% at very low N_{t0} (and low E; see Fig. 3a). Negative values mean that drop collisional processes tend to *decrease* evaporation, while positive values mean that they *increase* evaporation. For a given value of X_{l0}, a large concentration of drops means that the drops are small and that collision coalescence will dominate over collision breakup, resulting in the production of larger drops and negative Δ_c. On the other hand, a small N_{t0} means that the drops are larger, and that collision breakup will dominate, producing smaller drops and positive Δ_c. Thus, negative values suggest a

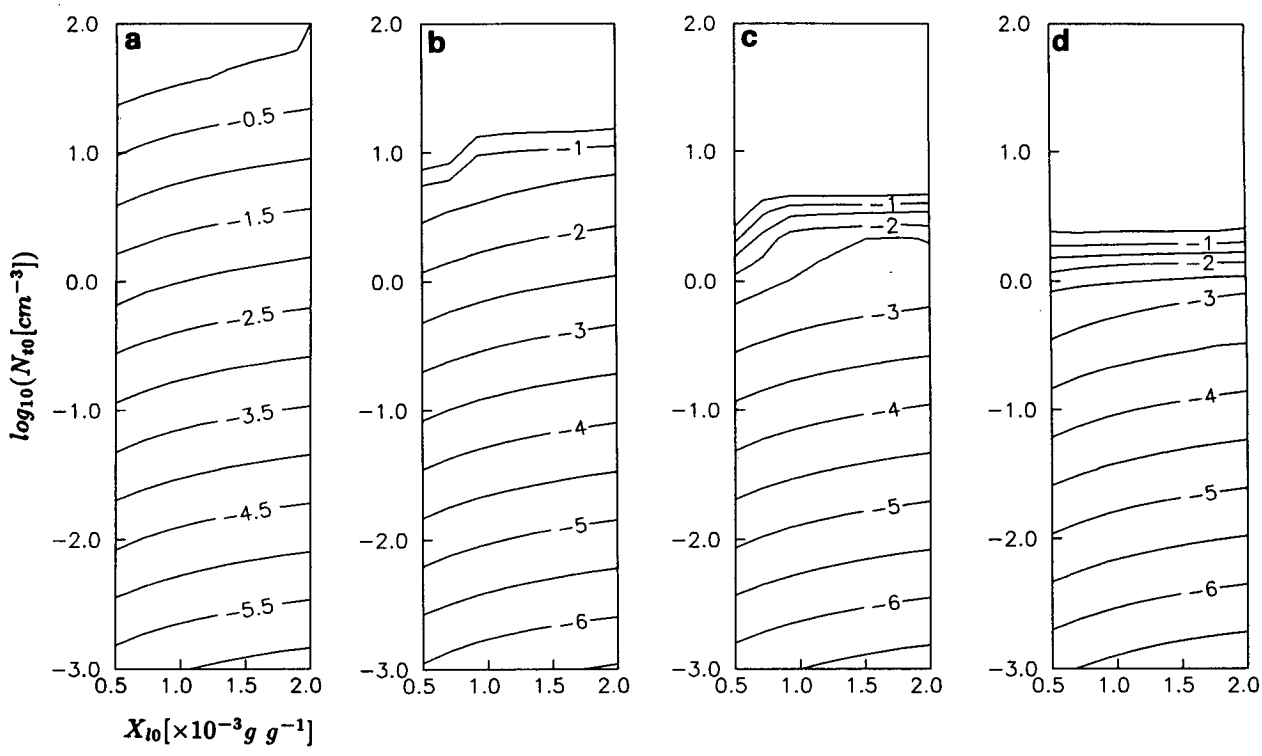

FIG. 7. Contours of Δ_T [defined by Eq. (13)] in (N_{t0}; X_{l0}) space for fall distances of (a) 500 m, (b) 1000 m, (c) 1500 m, and (d) 2000 m. The lapse rate of temperature is 8.5°C km^{-1}. Negative values imply that E increases as a result of the increase in cloud-base temperature from 5°C to 10°C.

balance of forces in favor of collision coalescence, while positive values suggest a balance in favor of collision breakup.

We note from these results that the error induced by neglecting collisional processes is of the order of a few percent and is thus of only secondary importance. Also, the magnitude of this effect is almost entirely a function of N_{t0} and h, and is virtually independent of X_{l0}.

4. Discussion

The results show that the proposed parameterization (PF) gives good estimates of E compared with those from the detailed model calculations for a wide range of situations. Results tend to improve for increasing values of fall distance h, lapse rate of temperature γ, and drop concentration N_{t0}: that is, conditions that are conducive to a high degree of evaporation. Although this parameterization has focused on only two cloud-base temperatures, T_b = 5°C or 10°C, the author is of the opinion that the difference in the results is small enough for interpolation to be viable for intermediate temperatures. The scheme could also be extended to temperatures outside of this range (warmer than 0°C) by generating the additional coefficients required by PF.

TABLE 3. The regression coefficients required by Eq. (12), that is, $E(X_{l0}, N_{t0}, h, \gamma) = a_0 X_{l0}^{a_1} N_{t0}^{a_2} h^{a_3} \gamma^{a_4}$ (excluding collisions) for T_b = 5°C and various lapse rates of temperature, γ. SEE is the standard error of estimate.

	All γ	γ = 7.5°C km^{-1}	γ = 8.5°C km^{-1}	γ = 9.5°C km^{-1}
a_0	0.0043	1.06	1.95	1.27
a_1	−0.0612	−0.0549	−0.0045	−0.0866
a_2	0.233	0.299	0.231	0.165
a_3	0.590	0.605	0.581	0.570
a_4	2.66			
SEE	15.9%	18.3%	12.6%	6.9%

a. *Implementation in a GCM*

The simple one-line algebraic equation given by Eq. (12) is easy to employ in a GCM, and requires negligible computational effort. The parameterization is formulated in terms of macroscopic variables, T_b, γ, and h, as well as microphysical variables, N_{t0} and X_{l0}.

1) MACROSCOPIC VARIABLES

The macroscopic variables required by (12) are either calculated (T_b, γ) or specified (h) by the GCM and present no problem.

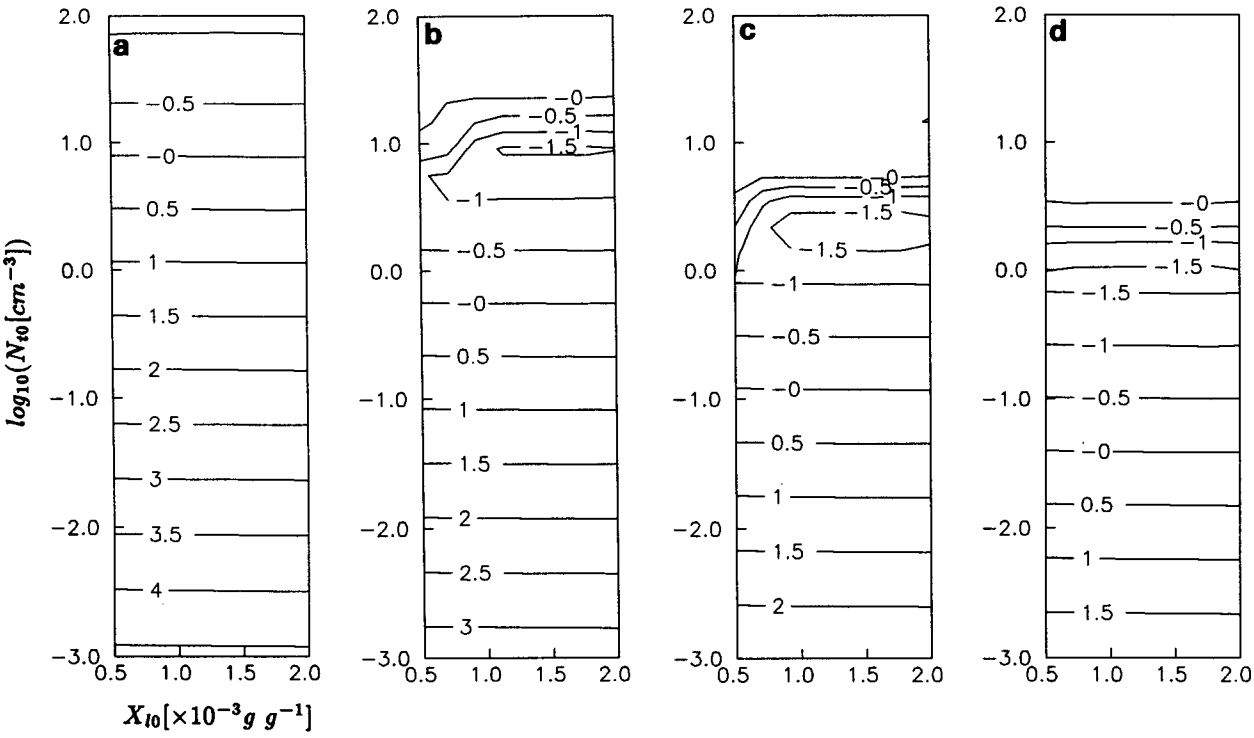

FIG. 8. Contours of Δ_c [defined by Eq. (14)] in (N_{t0}; X_{l0}) space for fall distances of (a) 500 m, (b) 1000 m, (c) 1500 m, and (d) 2000 m. The lapse rate of temperature is 8.5°C km^{-1}. Negative values imply that E increases as a result of the exclusion of drop collisions; positive values imply a decrease in E if drop collisions are excluded.

The model equations (1)–(5) represent a steady-state solution to an initial value problem. In this regard, two important issues need to be addressed.

(i) Steady-state solutions were typically achieved for simulated rainfall durations of about 15 minutes over the full 2-km fall distance and about 10 minutes for a 1-km fall distance. The steady-state assumption will be appropriate when the time required to reach steady state is less than the GCM resolvable time scale. Typical GCM time steps range between 15 and 30 minutes [e.g., the NCAR CCM1 (Hack et al. 1989) uses a time step of 18 minutes]. However, the resolvable time scale is a minimum of twice the time step (Haltiner and Williams 1980) so that GCMs typically resolve features on a time scale of 30–60 minutes. Thus, the results presented here are appropriate. A steady-state approach to cloud microphysics parameterizations for use in GCMs has also been used by Ghan and Easter (1992).

(ii) Although modified thermodynamic fields were generated during the course of a simulation, this was only for the purpose of correctly calculating drop evaporation, and not as a means of updating GCM fields. When including this parameterization in GCMs it should be borne in mind that the end product of PF is the estimate of E, and all adjustments to GCM fields (e.g., temperature and vapor) should be performed in a manner that is *self-consistent with the GCM equations.*

2) MICROPHYSICAL VARIABLES

At present, GCMs either predict or diagnose liquid water content (Smith 1990; Slingo 1987) but do not include information on drop concentrations. Specification of X_{l0} would be linked to the GCM-calculated values whereas N_{t0} would have to be determined on the basis of the rainfall type. Rainfall measurements using drop size spectrometers abound in the literature (e.g., Waldvogel 1974), and observationally based empirical relations relating drop concentrations to parameters such as rain rate I_0 have been calculated (e.g., Waldvogel 1974; Feingold and Levin 1986). These could be used to infer values of N_{t0} as follows. Empirical evidence (Feingold and Levin 1986) shows that

$$N_t = BI_0^b, \tag{15a}$$

and

$$\bar{r} = QI_0^q, \tag{15b}$$

where $\bar{r}$ is the average drop radius. Feingold and Levin found $B = 0.172\ 10^{-3}$, $b = 0.22$, $Q = 0.038$, and $q = 0.23$ (with I_0 [mm h^{-1}], N_t [cm^{-3}], and $\bar{r}$ [cm])

using a ground-based impaction distrometer (Joss and Waldvogel 1967) that measures drops in the range $0.017 \text{ cm} < r < 0.25 \text{ cm}$. The parameters B, b, Q, and q in (15) will depend primarily on rainfall type, geographical location, and the sizing range of the sampling instrument. (The aforementioned value of B is probably too low because it does not reflect the small and abundant drizzle drops.)

Assuming a lognormal form of the drop spectrum, we can write

$$X_l = C_1 N_t \bar{r}^3 \tag{16}$$

$$I_0 = C_2 N_t \bar{r}^{3.67} \tag{17}$$

where a constant drop spectrum breadth (Feingold and Levin 1986) has been assumed. We remind the reader that the subscript 0 in (15) and (17) implies $w' = 0$ in (10). (This is reasonable since the measurements were performed at the ground.) In (16) and (17), $C_1 = 6.15/\rho_a$ and $C_2 = 7.94 \times 10^8$ for ρ_a in g cm^{-3}, $\bar{r}$ in cm, X_l in g g^{-1}, and I_0 in mm h^{-1}. Using (15), (16), and (17), we can easily derive relations between N_t and X_l:

$$N_t = [BC_2^b (X_l/C_1)^{3.67b/3}]^{[1+(0.67b/3)]^{-1}} \tag{18a}$$

$$N_t = \left[\frac{(X_l/C_1)^{1/3([1/q]-3.67)}}{Q^{1/q} C_2}\right]^{\{1+1/3[(1/q)-3.67]\}^{-1}}. \tag{18b}$$

Either (18a) or (18b) can be used to close the PF parameterization scheme using observed values of B, b, Q, and q. This method of closure is not the only possible one; empirical relations other than (15) could just as easily be used. Direct empirical relationships between N_t and X_l would be even more straightforward to implement, and would not necessitate an assumption of the functional form of the drop spectrum. For example, Bower and Choularton (1992) have shown an approximately linear dependence of N_t on X_l in continental cumulus clouds.

As a means of calculating the sensitivity of calculations of E to errors in X_{l0} and N_{t0}, E was calculated using (12) in the range of X_{l0} and N_{t0} under consideration. These estimates can be directly calculated by differentiating (12) according to the chain rule. The results are graphically depicted by the contours in Fig. 9, which represent the relative error in E incurred by errors in X_{l0} of magnitude X_{l1}/X_{l2}. For example, if X_{l1} produces E_1 and X_{l2} produces E_2, then, all else being equal, the contours represent values of E_1/E_2. The results are for $h = 1000$ m, $\gamma = 8.5°\text{C km}^{-1}$, and $N_{t0} = 0.1 \text{ cm}^{-3}$. We see how a fourfold error in X_{l0} (that is, $X_{l1}/X_{l2} = 2\ 10^{-3}/0.5\ 10^{-3}$) results in an error in E of about 10%. Note that if E were expressed as an *absolute* quantity [that is, $X_{l0} - X_l(h)$] rather than a *normalized* quantity [Eq. (8)], then the errors in E would be approximately linearly dependent on the errors in X_{l0} (the coefficient a_1 is much smaller than unity).

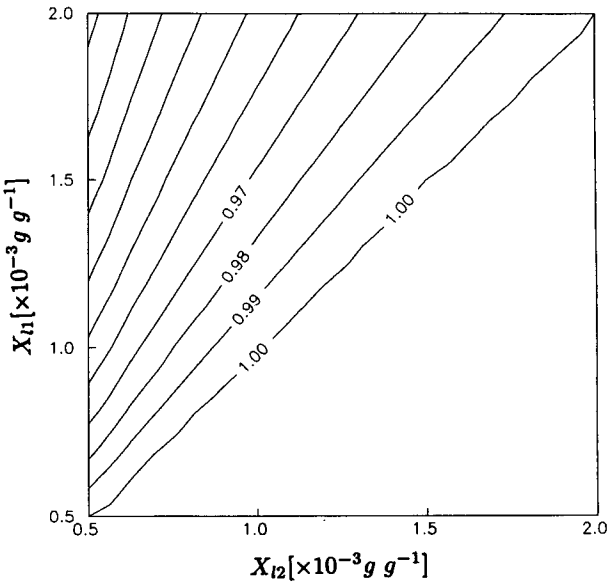

FIG. 9. Contours of E representing errors caused by overestimating X_{l0}. The contour values represent the degree of overestimation of E resulting from an overestimation of E by a factor X_{l1}/X_{l2}. The fall distance is set at 1000 m, the lapse rate at 8.5°C km^{-1}, and the drop concentration at 0.1 cm^{-3}.

Thus, errors in X_{l0} are potentially a significant source of error.

In Fig. 10 we change N_{t0} to investigate the attendant errors in E (h is fixed at 1000 m, γ at 8.5°C km^{-1}, and X_{l0} at 1×10^{-3}). Here we see a strong sensitivity of E to errors in N_{t0}; an order of magnitude error in N_{t0} (e.g., $N_{t1}/N_{t2} = 10^0/10^{-1}$) results in approximately 40% error in E, whereas a five order of magnitude error in N_{t0} creates an error in E of about 380%. The curves in Fig. 10 taper toward the vertical at $N_{t1} > 0$, because of the condition that $E \leq 100\%$.

3) EVAPORATION RATES

In GCMs it is necessary to calculate the amount of water evaporated over a certain time interval (e.g., one model time step). This can be done by calculating the time required for the rain to fall a distance h below cloud base with the aid of the average drop fall velocity $\bar{v}$, which is expressed in terms of the model variables:

$$\bar{v} = \delta \bar{r}^{\beta}, \tag{19}$$

with

$$\bar{r} = \left(\frac{3\rho_0 X_{l0}}{4\pi\rho_l N_{t0}}\right)^{1/3}. \tag{20}$$

The value of $\bar{r}$ remains approximately constant with height (e.g., Tzivion et al. 1989) and thus (20) is valid for $h > 0$. The coefficients δ and β have values dependent on $\bar{r}$; for $\bar{r} < 0.004$ cm, $\delta = 1.19 \cdot 10^4$, and

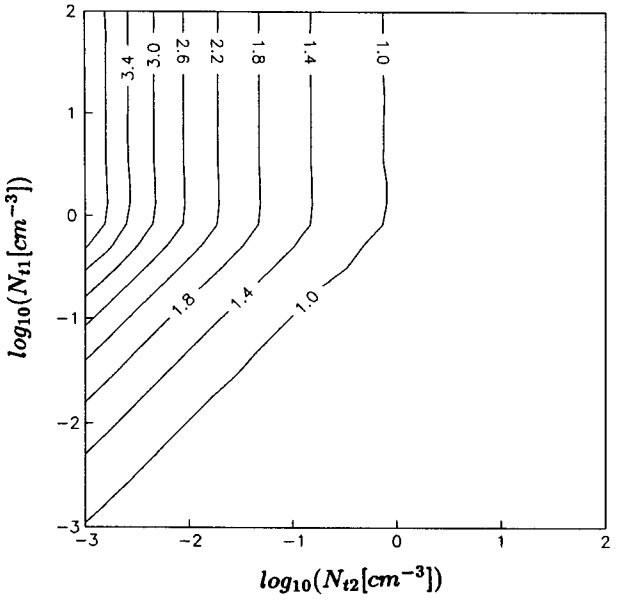

FIG. 10. Contours of E representing errors caused by overestimating N_{t0}. The contour values represent the degree of overestimation of E resulting from an overestimation of E by a factor N_{t1}/N_{t2}. The fall distance is set at 1000 m, the lapse rate at 8.5°C km^{-1}, and the mixing ratio at 1 10^{-3}.

$\beta = 2$; for $0.004 \leqslant \bar{r} < 0.06$ cm, $\delta = 80.0$, and $\beta = 1$; for $0.06 \leqslant \bar{r} < 0.2$ cm, $\delta = 20.1$, and $\beta = 0.5$; and for $\bar{r} \geqslant 0.2$ cm, $\delta = 9.17$, and $\beta = 0$ (e.g., Rogers and Yau 1989). Use of these coefficients gives $\bar{v}$ in m s^{-1}. Further accuracy can be achieved by adding the subgrid-scale vertical velocity calculated by the GCM parameterizations to $\bar{v}$. The time required for precipitation to fall a distance h is then given by

$$\tau = \frac{h}{\bar{v}}. \tag{21}$$

Use of (21) together with (12) enables calculations of evaporation *rates*.

b. *Error due to model assumptions*

1) ASSUMPTION OF ONE-DIMENSIONALITY

The model used in this study places great emphasis on microphysical calculations but assumes a simple one-dimensional dynamic framework. When parameterizations of the type used here are generated, many different model runs (of the order of hundreds) need to be performed and this precludes the use of two-dimensional models. Clearly, the vertical velocity, temperature, and vapor fields generated by the model are in error by some degree, and the evaporation calculations are in error by an amount that we will not attempt to ascertain. Indeed, two- and even three-dimensional models are abstractions of the real world, and the problem of verification remains central to studies of this nature. Remote measurements of rainfall using radar would be helpful in this regard (e.g., SOR), but they would still not resolve this issue because of their own inherent inaccuracies.

2) ENTRAINMENT OF ENVIRONMENTAL AIR

The model simulations have all assumed that turbulent diffusion is negligible. It is, however, quite possible to generate sets of parameterization coefficients that would include entrainment effects. The degree of entrainment (ENT) in one-dimensional models is usually crudely parameterized as being inversely proportional to a prescribed radius (R) of the rain shaft (e.g., Pruppacher and Klett 1978):

$$\text{ENT} = \frac{0.2}{R}. \tag{22}$$

The turbulent diffusion defined by (6) can be related to ENT (e.g., Srivastava 1985). The model could be run for a variety of R to make it more applicable to localized rainfall. We feel that the present status of cloud and rain parameterizations in GCMs is such that inclusion of entrainment is of secondary importance. If deemed necessary, further experiments of this nature, including entrainment effects, could be performed as a sequel to this study.

c. *Comparison with other works*

Sundqvist (1978) proposed a parameterization of evaporation based on the Kessler (1969) method. He suggested use of an equation in E_S of the form

$$E_S = k(1 - f)\bar{I}^{0.5} \tag{23}$$

where f is the saturation ratio in the subcloud layer, $\bar{I}$ is a height-integrated rainfall rate, and k is a constant that needs to be prescribed. (The subscript S is used because of differences in the definition of E; in the current work it is a normalized quantity whereas in Sundqvist's work it is not.) Because of the similarities in the forms of Eqs. (12) and (23), the scheme proposed by PF could provide a means of quantifying k. This would require an expression for the terminal velocity of the drops [Eq. (19)] in order to relate rain rate to liquid water mixing ratio. On the other hand, there appears to be little advantage in using (23) rather than (12), given the fact that the required coefficients have been quantified for different conditions.

As discussed in section 2c, SOR used an analytical framework to derive their parameterization scheme. This framework assumes that the falling drops have no influence on their environment and does not include dynamical–microphysical feedback mechanisms. They proposed an equation in E (E_{SOR}) of the form

$$E_{\text{SOR}}(h) = I_0(0) - I_0(h) = CI_0^{\alpha}(0)\Psi(h). \tag{9}$$

The units of E_{SOR} are [mm h^{-1}]. The parameters C and α were specified using radar data from convective rainfall measurements. Given the large errors in radar-derived rainfall measurements, the proposed PF scheme represents a viable alternative for calculating C and α. An attempt to derive these coefficients was made by calculating E_{SOR} using the present model and the definition of I used in (10). Thus, in these simulations, we have calculated (9) using I rather than I_0. This allows for a correct comparison of the model and radar data, since the latter were obtained for conditions of nonzero downdrafts. The results are depicted in Fig. 11, where we see that the model produces a family of curves (for different N_{t0}), each with very different C and α. Superimposed on these curves is the dashed line predicted by the radar measurements. Clearly one pair of average C and α values cannot capture the modeled variation in $E_{SOR}/\Psi(h)$. At low drop concentrations, there is a trend for the power-law form predicted by (9) to break down completely as downdrafts enhance the rain rate [see Eq. (10)] faster than evaporation is able to deplete it. To avoid the issue of downdraft-enhanced fluxes that are a feature of radar-derived rain rates, it is preferable to measure evaporation in terms of X_l rather than I.

5. Summary

A parameterization scheme representing the evaporation of rainwater below cloud base is presented and the coefficients required to quantify the evaporation are determined. The scheme is summarized as a simple empirical equation in terms of (i) cloud-base liquid mixing ratio, (ii) cloud-base drop concentration, (iii) distance of fall below cloud base, and (iv) lapse rate of temperature in the subcloud region. Two empirical equations are given, one for a cloud-base temperature of 5°C and the other for 10°C. The scheme is valid in the range of liquid water mixing ratios 0.5×10^{-3} g g^{-1} $< X_{l0} < 2 \times 10^{-3}$ g g^{-1}; drop concentrations 10^{-3} cm^{-3} $< N_{t0} < 10^2$ cm^{-3}; fall distances 20 m $< h <$ 2000 m; and lapse rates of 7.5°C $km^{-1} < \gamma <$ 9.5°C km^{-1}.

The results show that when compared to the detailed model calculations, the proposed parameterization provides good estimates of evaporation (usually within 20% and often within 10%) for a wide range of conditions. It is expected that the inclusion of such a scheme in GCMs will result in significant progress in the calculation of evaporation.

The results show that evaporation is mostly dependent on (i) the distance of fall below cloud base and (ii) the drop concentration (for a given liquid water mixing ratio). Accurate estimates of evaporation will require some estimate of the latter. It is suggested that observational studies of rainfall under different circumstances could provide an empirical relation between liquid mixing ratio and drop concentration. The method is based on detailed microphysical calculations of drop evaporation in a one-dimensional numerical model [Eqs. (1)–(5)] in which pressure perturbation forces and entrainment were neglected. Future work will include entrainment effects in the calculations. In addition, efforts are currently under way to compare and contrast the parameterization results with measurements from new millimeter-wavelength Doppler radar systems.

Acknowledgments. The author wishes to thank Dr. Jin-Luen Lee of Science and Technology Corporation, Virginia, for helpful discussions.

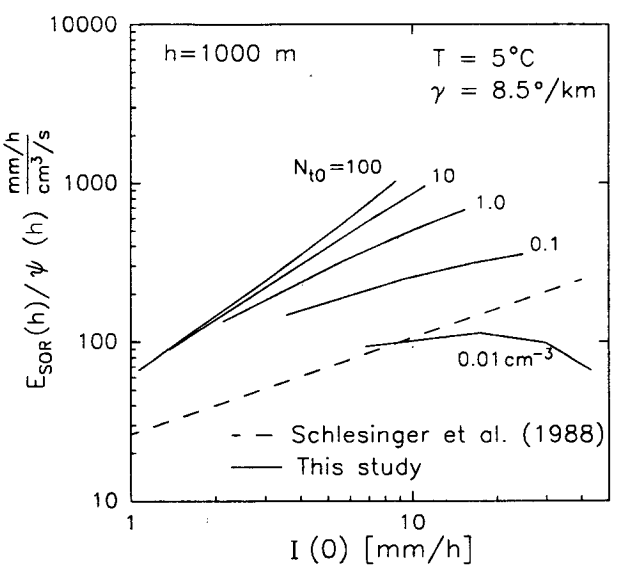

FIG. 11. Curves showing the function E_{SOR}/Ψ [defined by Eq. (9)] as a function of rainfall rate at cloud base [$I(0)$]. The parameterization of Schlesinger et al. (1988) predicts a power-law relation between these parameters (the dashed line). The figure shows how the values of the power-law fit will vary considerably with variation in drop concentration at cloud base. At low concentrations, the power law breaks down as the increase in rain rate associated with downdraft enhancement overcomes the decrease in rain rate due to evaporation. See text for discussion.

APPENDIX

Definitions of Parameters Used in the Model Equations

c_p	the specific heat at constant pressure
D	the advection operator
Δz	the vertical grid dimension
Δ_c	see Eq. (14)
Δ_T	see Eq. (13)
E	the subcloud evaporation defined by (8)
f	the saturation ratio below cloud base
F	the turbulence operator
ϕ	an arbitrary quantity
g	gravitational acceleration
γ	the lapse rate of temperature below cloud base
$\Gamma_{\theta 0}$	the vertical lapse rate of the virtual potential

	temperature of the unperturbed atmosphere
Γ_{q0}	the vertical lapse rate of the specific humidity in the unperturbed atmosphere
h	fall distance below cloud base, defined as $h = 0$
I	rain rate [Eq. (10)]
I_0	rain rate [Eq. (10) with $w' = 0$]
$\bar{I}$	vertically integrated rain rate
K	the eddy mixing coefficient
L	the latent heat of condensation
$n(r)dr$	the number of drops per unit volume with radii between r and $r + dr$
N_k, M_k	the number and mass concentration in a bin k
N_t	the total number concentration of drops (cm^{-3})
N_{t0}	the total number concentration of drops at cloud base (cm^{-3})
P	the pressure
P_0	the ground pressure
q'_v	the perturbation of the specific humidity
r	drop radius
R	the radius of the rain shaft
R_d	the gas constant for dry air
ρ_0	the density of the unperturbed atmosphere
ρ_l	the density of liquid water
t	time
τ	time required for rain to fall distance h
T_b	cloud-base temperature
T_{v0}	the virtual temperature of the unperturbed atmosphere
θ'_v	the perturbation of the virtual potential temperature
θ_{v0}	the virtual potential temperature of the unperturbed atmosphere
$v(r)$	the terminal velocity of a drop of radius r (defined as positive downwards)
$\bar{v}$	the average terminal velocity of drop spectrum (defined as positive downwards)
w'	the subgrid-scale vertical velocity component (defined as positive upwards)
X_l	the liquid water mixing ratio ($g\ g^{-1}$)
X_{l0}	the liquid water mixing ratio at cloud-base ($g\ g^{-1}$)
z	the vertical coordinate (height above ground)

REFERENCES

Bower, K. N., and T. W. Choularton, 1992: A parameterisation of the effective radius of ice-free clouds for use in global climate models. *Atmos. Res.*, **27,** 305–339.

Browning, K. A., 1990: Rain, rainclouds and climate. *Quart. J. Roy. Meteor. Soc.*, **116,** 1025–1051.

Committee on Earth Sciences: 1989: Our Changing Planet: The FY1990 U.S. Global Change Research Program, U.S. Geological Survey, Reston, Va., 118 pp.

Cess, R. D., G. L. Potter, J. P. Blanchet, G. J. Boer, S. J. Ghan, J. T. Kiehl, H. Le Treut, Z.-X. Li, X.-Z. Liang, J. F. B. Mitchell, J.-J. Morcrette, D. A. Randall, M. R. Riches, E. Roeckner, U. Schlese, A. Slingo, K. E. Taylor, W. M. Washington, R. T. Wetherald, and I. Yagai, 1989: Interpretation of cloud–climate feedback as produced by 14 atmospheric general circulation models. *Science,* **245,** 513–516.

Clark, T. L., and R. List, 1971: Dynamics of a falling particle zone. *J. Atmos. Sci.*, **28,** 718–727.

Feingold, G., and Z. Levin, 1986: The lognormal fit to raindrop spectra from frontal convective clouds in Israel. *J. Climate Appl. Meteor.*, **25,** 1346–1363.

——, and A. J. Heymsfield, 1992: Parameterizations of condensational growth of droplets for use in general circulation models. *J. Atmos. Sci.*, **49,** 2325–2342.

——, S. Tzivion, and Z. Levin, 1991: The evolution of raindrop spectra. Part III: Downdraft generation in an axisymmetrical model. *J. Atmos. Sci.*, **48,** 315–330.

Ghan, S. J., and R. C. Easter, 1992: Computationally efficient approximations to stratiform cloud microphysics parameterization. *Mon. Wea. Rev.*, **120,** 1572–1582.

Girard, C., and R. List, 1975: The thermodynamics of falling particle zones. *Pure Appl. Geophys.*, **113,** 1035–1053.

Haltiner, G. J., and R. T. Williams, 1980: *Numerical Prediction and Dynamic Meteorology, 2d ed.* Wiley, 477 pp.

Hack, J. J., L. M. Bath, G. S. Williamson, and B. A. Boville, 1989: Modifications and Enhancements to the NCAR Community Climate Model (CCM1). NCAR Tech. Note, NCAR/TN-336+STR, 144 pp.

Harris, F. I., 1977: The effects of evaporation at the base of warm precipitation layers: Theory and radar observations. *J. Atmos. Sci.*, **34,** 651–672.

Joss, J., and A. Waldvogel, 1967: Ein spektrograph fur niederschlagstrophen mit automatischer auswertung. *Pure Appl. Geophys.*, **68,** 240–246.

Kamburova, P. L., and F. H. Ludlam, 1966: Rainfall evaporation in thunderstorm downdraughts. *Quart. J. Roy. Meteor. Soc.*, **92,** 510–518.

Kessler, E., 1969: On the distribution and continuity of water substance in atmospheric circulation. *Meteor. Monogr.*, **10,** Amer. Meteor. Soc., 84 pp.

Levin, L. M., 1954: Size distribution function for cloud droplets and rain drops. *Dokl. Akad. Nauk. SSSR,* **94,** 1045–1053.

Levin, Z., G. Feingold, S. Tzivion, and A. Waldvogel, 1991: The evolution of raindrop spectra: Comparisons between modeled and observed spectra along a mountain slope in Switzerland. *J. Appl. Meteor.*, **30,** 893–900.

Mitchell, J. F. B., C. A. Senior, and W. J. Ingram, 1989: CO_2 and climate: A missing feedback? *Nature,* **341,** 132–134.

Proctor, F. H., 1988: Numerical simulations of an isolated microburst. Part I: Dynamics and structure. *J. Atmos. Sci.*, **45,** 3137–3160.

Pruppacher, H. R., and J. D. Klett, 1978: *Microphysics of Clouds and Precipitation.* D. Reidel, 714 pp.

Rogers, R. R., and M. K. Yau, 1989: *A Short Course in Cloud Physics, third ed.* Pergamon, 293 pp.

Schlesinger, M. E., J. H. Oh, and D. Rosenfeld, 1988: A parameterization of the evaporation of rainfall. *Mon. Wea. Rev.*, **116,** 1887–1895.

Slingo, J. M., 1987: The development and verification of a cloud prediction scheme for the ECMWF model. *Quart. J. Roy. Meteor. Soc.*, **113,** 899–927.

Smith, R. N. B., 1990: A scheme for predicting layer clouds and their water content in a general circulation model. *Quart. J. Roy. Meteor. Soc.*, **116,** 435–460.

Sundqvist, H., 1978: A parameterization scheme for non-convective condensation including prediction of cloud water content. *Quart. J. Roy. Meteor. Soc.*, **104,** 677–690.

Srivastava, R. C., 1985: A simple model of evaporatively driven downdraft: Application to microburst downdraft. *J. Atmos. Sci.*, **42,** 1004–1023.

Tzivion, S., G. Feingold, and Z. Levin, 1989: The evolution of raindrop spectra. Part II: Collisional collection/breakup and evaporation in a rainshaft. *J. Atmos. Sci.*, **46,** 3312–3327.

Waldvogel, A., 1974: The N_0 jump of raindrop spectra. *J. Atmos. Sci.*, **31,** 1067–1078.